SCIENTIFIC REPORTS

OPEN

Efficient nitrogen incorporation in ZnO nanowires

Jan E. Stehr[1], Weimin M. Chen[1], Nandanapalli Koteeswara Reddy[2], Charles W. Tu[3] & Irina A. Buyanova[1]

Received: 25 March 2015
Accepted: 17 July 2015
Published: 24 August 2015

One-dimensional ZnO nanowires (NWs) are a promising materials system for a variety of applications. Utilization of ZnO, however, requires a good understanding and control of material properties that are largely affected by intrinsic defects and contaminants. In this work we provide experimental evidence for unintentional incorporation of nitrogen in ZnO NWs grown by rapid thermal chemical vapor deposition, from electron paramagnetic resonance spectroscopy. The incorporated nitrogen atoms are concluded to mainly reside at oxygen sites (N_O). The N_O centers are suggested to be located in proximity to the NW surface, based on their reduced optical ionization energy as compared with that in bulk. This implies a lower defect formation energy at the NW surface as compared with its bulk value, consistent with theoretical predictions. The revealed facilitated incorporation of nitrogen in ZnO nanostructures may be advantageous for realizing p-type conducting ZnO via N doping. The awareness of this process can also help to prevent such unintentional doping in structures with desired n-type conductivity.

ZnO has a wide and direct band gap (~3.3 eV at room temperature) and a large exciton binding energy (60 meV at room temperature). It can be easily synthesized in both bulk, single-crystal form and also in a diverse group of nanostructure morphologies. In addition, this material is nontoxic, sustainable and cheap. These attributes make ZnO a very promising material for a wide variety of applications including photonics, electronics, sensing and energy harvesting[1–5]. In particular, one-dimensional ZnO nanowires (NWs) have recently attracted a substantial scientific and technological interest for realization of gas sensors and ultraviolet (UV) optoelectronic devices, such as light emitting diodes (LEDs), solar cells, and photo detectors[5–8]. All these applications, however, require a good understanding and precise control of optical and electrical properties of the material that are known to be largely affected by intrinsic defects and impurities. Zinc vacancies (V_{Zn}) for instance, which have the lowest formation energy among all intrinsic defects in n-type ZnO[9–11], can form detrimental complex centers with group III donors (e.g. Al), thus limiting the n-type doping efficiency[12–14]. On the other hand, they can also facilitate energy upconversion in ZnO[15,16], attractive for photovoltaic applications. Therefore, depending on the intended outcome, defects can be vital or fatal[17,18].

Another group of defects that are important for understanding electrical properties of ZnO involve defects containing nitrogen atoms. Nitrogen has been long considered as one of the most promising candidates for p-type doping in ZnO. Interestingly, even though it has already been proven that nitrogen substituting for oxygen (N_O)[19–23] does not create a shallow acceptor state, p-type ZnO using nitrogen as a dopant has been commonly reported[24–26]. So far, it is still under discussion how nitrogen doping leads to the formation of shallow acceptors in ZnO. Here one needs to keep in mind that the doping processes can be largely affected not only by growth conditions and type/concentration of the utilized dopants, but also residual contamination of the source material or even the background gases in the growth chamber[27]. For example, it was reported that p-type conductivity in ZnO could be promoted in nanostructured materials[25,28,29]. Though the exact physical mechanism responsible for this effect remains

[1]Linköping University, Department of Physics, Chemistry and Biology, Linköping, 581 83, Sweden. [2]Humboldt University, Institute of Chemistry, Berlin, 12489, Germany. [3]University of California, Department of Electrical and Computer Engineering, La Jolla, CA 92093, USA. Correspondence and requests for materials should be addressed to J.E.S. (email: janst@ifm.liu.se) or I.A.B. (email: iribu@ifm.liu.se)

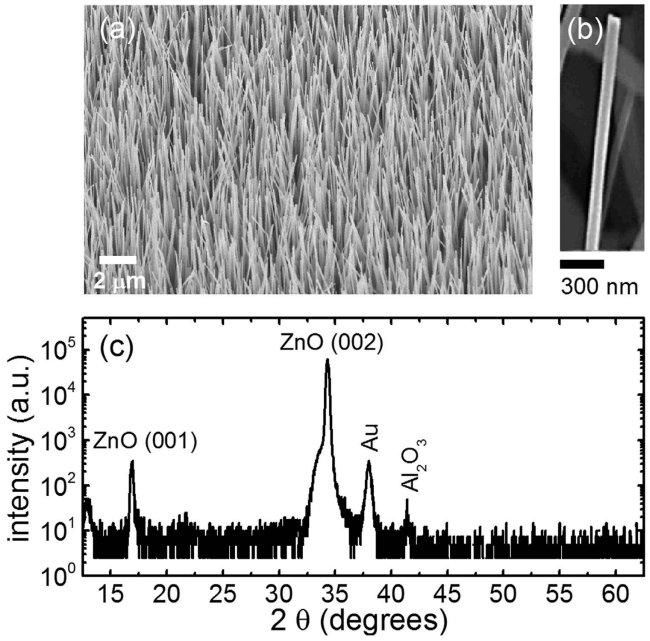

Figure 1. (**a**) An SEM overview image of the studied ZnO NWs under a tilted view of 45°. (**b**) a magnified SEM image of a single ZnO NW. (**c**) XRD diffractogram of the studied ZnO NWs.

unknown, it could be caused by formation of complexes with residual defect/impurities. Indeed, the energy level of the N acceptor can be affected by its local surrounding[30], complexing with residual group III impurities[31] and defects[32,33], as well as formation of N-N molecules[34]. Moreover, growth conditions utilized during the NW growth may facilitate dopant incorporation leading to higher dopability of these materials. In this letter we employ magnetic resonance spectroscopy[35] to investigate defect formation processes in nominally undoped ZnO NWs grown by chemical vapor deposition, aiming to single out chemical origin of incorporated contaminants.

Results and Discussion

Figure 1(a) shows a representative scanning electron microscopy (SEM) image of the investigated ZnO NWs. A magnified image from a single NW is shown in Fig. 1(b). Most of the NWs are found to be vertically aligned along the crystallographic [0001] axis and exhibit a uniform size distribution with an average length and diameter of 30 μm and 100 nm, respectively. Some of the NWs are, however, randomly tilted by up to 20°. The excellent structural quality was further confirmed from performed x-ray diffraction (XRD) experiments, The XRD spectra of the ZnO NWs contain four peaks which can be assigned to ZnO (001) and (002) reflexes, Au and Al_2O_3 - see Fig. 1(c). The latter two reflexes are expected since the NWs were grown on an Al_2O_3 substrate and Au was used as a catalyst. The XRD results confirm that the NWs are preferentially oriented along the crystallographic c-axis ([0001] direction), since the calculated d-spacing of the major reflex ($2\theta = 34.4°$, $d = 0.261$ nm) matches that expected for hexagonal ZnO. The full width at half maximum (FWHM) of the main ZnO reflex was found to be 0.27°, indicative of the high quality ZnO.

Figure 2 depicts EPR spectra of the ZnO NW arrays measured in dark (a) and under white light illumination (b). In the dark, two single-line EPR signals labeled as A and B in Fig. 2 can be observed. White light illumination leads to appearance of another EPR signal (labeled as C) that consists of three equally spaced lines, which is characteristic for a resolved hyperfine interaction involving a nucleus spin $I = 1$ with natural abundance of 100%.

In order to identify the observed EPR signals we performed angular dependent measurements under light illumination by rotating the sample from an orientation with the NWs aligned parallel to a static magnetic field (**B**), i.e. $\Theta = 0°$, towards $\Theta = 90°$. In the latter case **B** is oriented perpendicularly to the [0001] NWs axis. Figure 3(a) shows representative results from these measurements, taking as an example EPR spectra measured with Θ of 10°, 70° and 90°. An anisotropic behavior for signals B and C can be clearly observed, while signal A is isotropic. By using a spin-Hamiltonian operator in the form of

$$\mathcal{H} = \mu_B \boldsymbol{BgS} + \boldsymbol{SAI} - g_N \mu_N \boldsymbol{BI}, \quad (1)$$

i.e. including the Zeeman energy (the first term), the hyperfine interaction (the second term) and the nuclear Zeeman interaction (the third term), we can determine spin-Hamiltonian parameters of the observed EPR signals. Here we neglect the quadrupole interaction for nuclei with $I > 1/2$, since the EPR

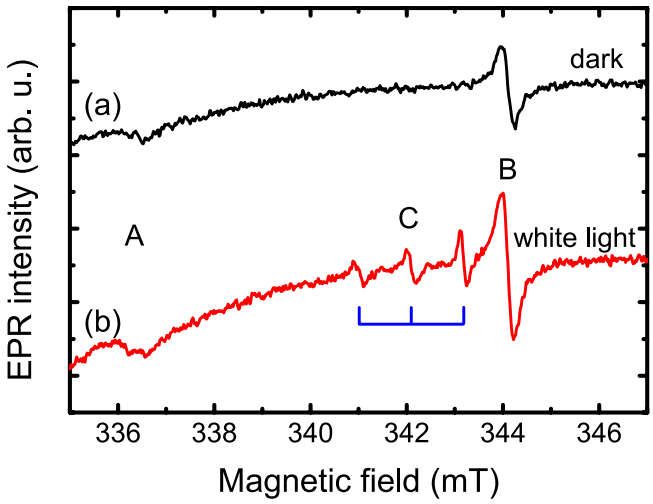

Figure 2. EPR spectra of the studied ZnO NWs measured at 4 K and a microwave frequency of 9.4 GHz in the dark (**a**) and under white light illumination (**b**) with an applied magnetic field rotated away from the NW growth axis ([0001], i.e. the c - axis) by $\Theta = 70°$.

signal intensity of the forbidden transitions arising from the quadrupole interaction is too weak to determine its interaction tensor. It is found that signal A has an electron spin $S = 1/2$ and an isotropic g-value of 2.002. Within the experimental error, this value is identical to the free electron g-value $g_e = 2.0023$. We, therefore, assign this signal to dangling bonds on the surface of the NWs[36,37], which seems to be very likely considering a large surface-to-volume ratio in the NWs. Signal B has an electron spin $S = 1/2$ and a slightly anisotropic g-tensor with $g_{||} = 1.957$ and $g_{\perp} = 1.955$ (see Fig. 3(c)), where parallel and perpendicular orientations are given with respect to the crystallographic c-axis. Such g-values are typical for shallow effective mass donors in ZnO[35]. Judging from the determined g-values, this shallow donor is most likely caused by unintentionally incorporated hydrogen[38]. Unfortunately the corresponding hyperfine interaction (1.4 MHz) is too small to be resolved in the X-band EPR experiments conducted in this work.

Let us now discuss the chemical origin of signal C. First of all we note that it must arise from a chemical element that has an isotope with a nuclear spin $I = 1$ and nearly 100% natural abundance. The only element in the periodic table which satisfies this requirement is nitrogen as the ^{14}N isotope has $I = 1$ and 99.6% natural abundance. Moreover, signal C exhibits strongly anisotropic behavior with an angular dependent g-value and the hyperfine interaction parameter A. This can also be seen from Fig. 3(b) where the dependence of signal C on the orientation of the external magnetic field is depicted. By fitting the experimental data with the spin-Hamiltonian given by Eq. (1) we obtain $g_{||} = 1.996$, $g_{\perp} = 1.963$, $A_{||} = 82.3$ MHz and $A_{\perp} = 9.7$ MHz. The determined spin-Hamiltonian parameters are very similar to those reported in the literature for the substitutional N_O center in bulk ZnO[20,39]. We therefore identify signal C as arising from a nitrogen atom substituting oxygen. In bulk, a typical linewidth ΔB of the N_O EPR lines is about 0.03 mT and slightly deviates between the lines, which can be explained by inhomogeneity of the g-values and hyperfine interaction[39]. An additional broadening (up to 0.2 mT) of the C lines in the studied NWs is likely caused by imperfect perpendicular alignments of the NWs relative to the substrate surface, evident from their random tilt directions and angles up to 20° from the vertical direction as revealed from the performed scanning electron microscopy measurements[40].

The energy level position of the N_O center in the ZnO NWs can be determined from photo-EPR measurements. The measured spectral dependence of the N_O EPR signal on the excitation photon energy is shown by the open circles in Fig. 4(a). We can see that the N_O center can be converted into its paramagnetic state N_O^0 only when the photon energies exceed 1.75 eV. The recharging process can be further understood by analyzing temporal behavior of the N_O signal after switching on the light. The corresponding results are shown in Fig. 4(b), where the y-axis displays the difference of the measured EPR intensity (I) from the saturation value (I_∞) shown in a logarithmic scale. The linear slope shown by the solid line indicates a mono-exponential process due to direct recharging of the studied center without involvement of other defects. Moreover, since light illumination within the same spectral range also causes an increase of the shallow donor EPR signal (see Fig. 2), the recharging process results in photo-ionization involving the conduction band. This means that the light-induced conversion of the N_O center into its paramagnetic charge state occurs as a result of the process

$$N_O^- + h\nu \rightarrow N_O^0 + e_{CB}^-, \tag{2}$$

as schematically shown in Fig. 4(c).

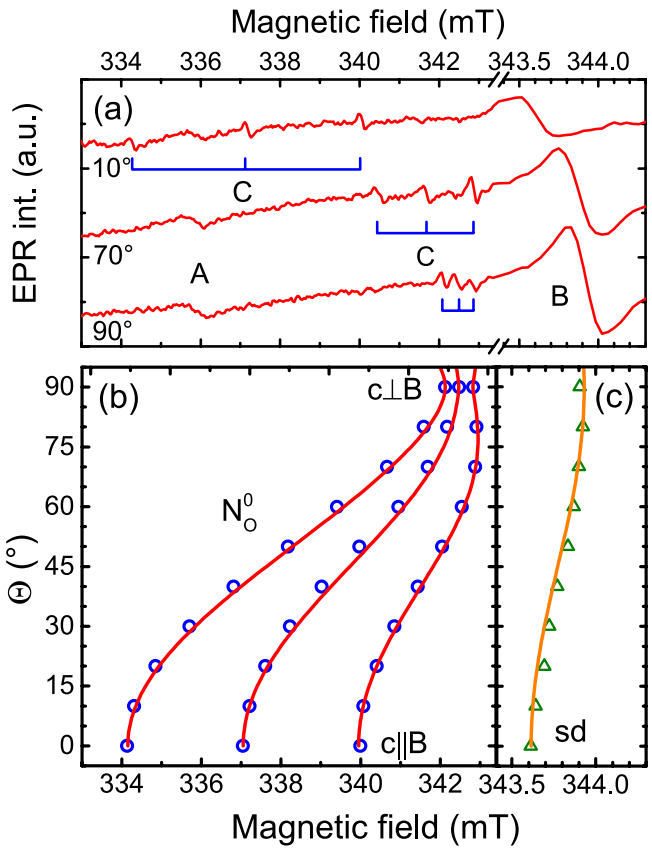

Figure 3. (**a**) EPR spectra of the ZnO NWs measured at 4 K under white light illumination with an applied magnetic field rotated away from the NW growth axis ([0001], i.e. the c - axis) by $\Theta = 10°$, 70° and 90°. (**b**) Angular dependent plot of the N_O EPR field positions (the open circles) and the best fit using the spin-Hamiltonian described in the text (the solid lines). (**c**) Anisotropic behavior of signal B, i.e. the shallow donor (sd) EPR field postions (the open triangles) obtained by rotating a magnetic field direction from B parallel to c to B perpendicular to c. The solid line is the best fit obtained by using the spin-Hamiltonian described in the text. (Note different x-axis scales in (**b**,**c**)).

It is interesting to note that the photo-ionization threshold energy in the NWs differs from that in bulk ZnO where the threshold energy is found to be at around 2 eV (see the dashed curve in Fig. 4(a)), which is in agreement with previous reports[20]. One possible explanation for this deviation is that, unlike in bulk ZnO, the N_O centers in the NWs are not distributed uniformly through the volume but are located in proximity to the NW surface. (The possibility of the N_O centers to be directly located on the NW surface can be excluded, however, since this would drastically alter the spin-Hamiltonian parameters of the centers, which is not the case). In fact previous theoretical studies[41,42] have concluded that the ionization energies of donor and acceptor impurities are strongly enhanced in nanowires with respect to their values in bulk. Moreover, due to surface band bending[43] optical ionization of the N_O^- center within the near-surface region can occur not only due to spatially direct, but also spatially indirect optical transitions. In addition, the electron-phonon interactions for the N_O^- center, which significantly affect the photoionization edge, could be altered in the proximity to the surface. Both effects will lead to an overall broadening of the ionization edge, as is observed experimentally. This suggestion is also consistent with the theoretical results of Gutjahr *et al.*[44] and Haffad *et al.*[45], which predicted that incorporation of nitrogen in ZnO is more energetically favorable at (or close to) the surface than in volume regions. This is expected to result in a higher efficiency of N doping in nanostructures with a high surface-to-volume ratio. Gutjahr *et al.*[44] have explained the decrease in the formation energy by charge transfer between Zn dangling bonds on the surface and the N_O impurities. Existence of such dangling bonds on the surface of the studied NWs is indeed confirmed by the observation of signal A in our EPR measurements.

Of course the formation energy of N_O in bulk and nanostructured ZnO is dependent on the growth conditions (O-rich or Zn-rich) and the Fermi level position, which is strongly affected by the dopant concentration. However, these dependencies are known from ab initio density functional theory (DFT) calculations[22,23]. For examples, the formation energy scales linearly with the Fermi level position (determined by the dopant concentration) under fixed growth conditions (Zn- or O-rich), since effects of

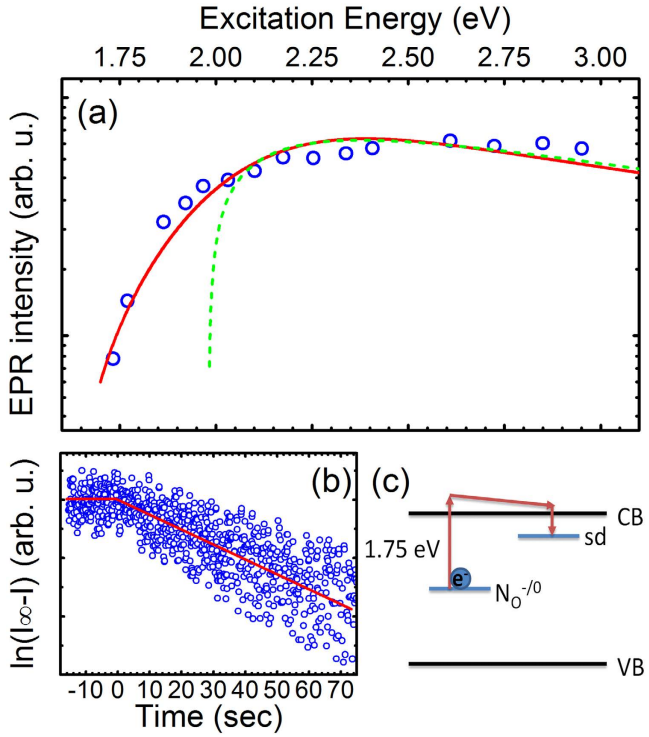

Figure 4. (**a**) EPR intensity of the N_O signal (open circles) as a function of the light excitation energy for the studied ZnO NWs and bulk ZnO (dashed line). The solid line is a guide to the eye. (**b**) Time dependent behavior of the N_O signal after switching on the light. The y-axis displays the difference of the measured EPR intensity (I) from the saturation value (I_∞) shown in a logarithmic scale. The linear slope shown by the solid line indicates a mono-exponential process due to direct recharging. (**c**) Illustration of the N_O photo-EPR recharging process. The notation "sd" denotes the shallow donor center.

lattice relaxation at doping concentration lower than 6.06% are negligible[45]. Therefore, our conclusion of the reduced formation energy of the N_O centers in the NWs, though obtained for low-doped ZnO, should remain valid even for higher doping concentrations.

The remaining and somewhat puzzling questions are what are the sources and mechanism responsible for the revealed unintentional doping of the ZnO NWs by nitrogen. The studied structures were grown by chemical vapor deposition in an Ar ambient using gold as a catalyst. Therefore, nitrogen atoms were most likely supplied by contaminations in the used Ar_2 and O_2 source gases and/or by residual background N_2 gas. Both source gases had a purity of 6N (99.9999%) and hence can contain up to 1 ppm N_2. The contamination of the residual background gas most likely stems from venting the growth chamber with N_2 gas after the deposition of the gold catalyst on the sapphire substrate prior to the growth of the NWs. We believe that the N_2 contamination from the used Ar_2 and O_2 source gases dominates, since defect incorporation due to contaminations of the used source gases is a known phenomenon in RTCVD processes[46,47] and was shown to prevail over contamination by residual chamber background gases[46]. According to previous studies[27,48], nitrogen molecules can be dissolved easily in molten metals and subsequently split into atomic nitrogen. This process happens when metal is heated to high temperatures ($T_{Growth} = 950\,°C$) under the presence of molecular nitrogen gas. Under these conditions nitrogen molecules permeate into the metal and nitridation proceeds by dissociation of nitrogen molecules and absorption of nitrogen atoms by the metal[48]. Taking into account the large surface area of the gold catalyst during the growth, this process can be rather efficient. The dissolved atomic nitrogen could then incorporate and diffuse (comment: diffusion may happen but is not necessary, as the Au droplet is floating on the surface of the growing NWs) into the growing NWs and predominantly reside at oxygen sites giving rise to the N_O EPR signal. An illustration of the suggested process of nitrogen incorporation into the ZnO NWs is shown in Fig. 5. We would like to note that considering a limited amount of nitrogen in the growth chamber (only a few ppm), the dopant incorporation efficiency during the revealed doping process must be very high. Indeed, the concentration of the N_O centers estimated based on the EPR signal intensity is about $2–4 \times 10^{16}\,cm^{-3}$, which is only by about one order of magnitude lower than the deduced concentration of the residual shallow donors (signal B) of $2–4 \times 10^{17}\,cm^{-3}$ in the NWs. The low formation energy of the substitutional nitrogen center in ZnO nanostructures is advantageous for the synthesis of p-type conductive via nitrogen doping, e.g. due to N-containing defect complexes or nitrogen molecules. The awareness of this process can also help to prevent such unintentional doping in

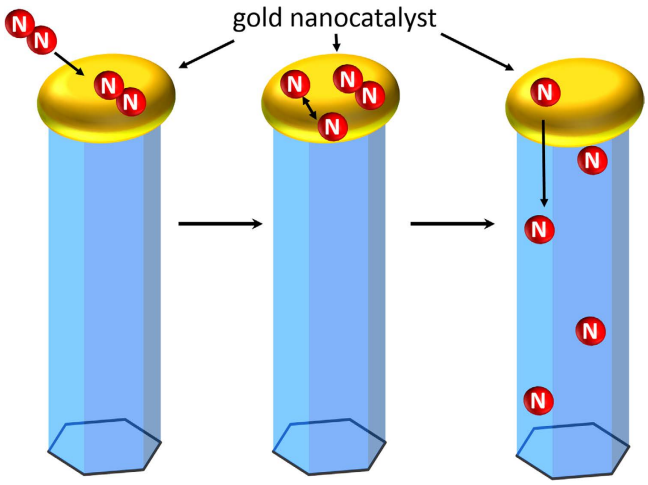

Figure 5. Schematic illustration of the nitrogen incorporation into the ZnO NWs from the residual background gases in the growth chamber that contain N_2.

structures where n-type conductivity is desired, as N_O can act as a compensation center in n-type ZnO. Unfortunately, it is not possible to directly compare the efficiency of the N_O incorporation during the employed growth with that achieved previously in intentionally N-doped ZnO NWs, since the information on the N concentration in the wires was not provided in most of the earlier reports[27,49,50]. Yuan *et al.*[24] estimated that the carrier concentration in their N-doped ZnO NWs grown by chemical vapor deposition (CVD) is $\sim 1 \times 10^{18}\,cm^{-3}$. However, the exact configuration of the incorporated nitrogen (N_O, N-molecules or N-complexes) and its concentration were not determined.

Conclusion

In summary, we have provided an unambiguous experimental proof for efficient unintentional doping with nitrogen in ZnO NWs during the RTCVD growth process. Based on our results from the detailed EPR measurements, incorporated nitrogen is shown to reside at oxygen sites forming a substitutional N_O acceptor. Based on the lower photo-ionization threshold energy of the N_O center in the ZnO NWs as compared with its value in bulk ZnO, the defect is suggested to be located in proximity to the surface. This assumption is consistent with theoretical predictions[44,45] of enhanced N incorporation at or close to the ZnO surface. The revealed doping process is shown to be very efficient leading to a rather high concentration ($\sim 2–4 \times 10^{16}\,cm^{-3}$) of unintentional N dopants in the NWs even from the contamination by the source and background gases. Our finding thus underlines the importance of controlling such background contamination as compensation by the N_O acceptors may hinder achieving high n-type conductivity in nanostructured ZnO. On the other hand, the lowered formation energy of N_O in NWs might be beneficial for achieving p-type conducting ZnO nanostructures via nitrogen doping, e.g. due to N-containing defect complexes or nitrogen molecules.

Methods

The ZnO NWs were grown on gold coated c-plane sapphire substrates by using rapid thermal chemical vapor deposition (RTCVD). The growth was performed at a growth temperature of 950 °C under pressure of 20 Torr with Ar_2 and O_2 flows of 100 and 2 sccm, respectively[40]. The Au catalyst had a thickness of about 3 nm and was deposited using e-beam evaporation. Most of the NWs are vertically aligned along the crystallographic [0001] axis and exhibit a uniform size distribution with an average length and diameter of 30 μm and 100 nm, respectively. Some of the NWs are, however, randomly tilted by up to 20°.

EPR experiments were performed at a microwave frequency of 9.4 GHz (X-band) at a temperature of 4.2 K. To perform photo-EPR measurements, a Xenon lamp was used as an excitation source. Appropriate long-pass and short-pass filters were utilized to select specific illumination wavelengths whereas neutral density filters were inserted to ensure the same excitation power at all chosen wavelengths. To avoid effects of ambient illumination and to guarantee the same initial conditions, the sample was cooled down each time in the dark before illumination. Time-dependent photo-EPR measurements were performed at a constant magnetic field corresponding to the EPR peak position and the EPR signal strength was monitored as a function of time after switching on the light.

References

1. Özgür, U. *et al.* Comprehensive Review of ZnO Materials and Devices. *J. Appl. Phys.* **98,** 41301 (2005).
2. Pearton, S. J. & Ren, F. Advances in ZnO-Based Materials for Light Emitting Diodes. *Curr. Opin. Chem. Eng.* **3,** 51–55 (2014).
3. Xiong, H.-M. ZnO Nanoparticles Applied to Bioimaging and Drug Delivery. *Adv. Mater.* **25,** 5329–5335 (2013).

4. Jing, Z. & Zhan, J. Fabrication and Gas-Sensing Properties of Porous ZnO Nanoplates. *Adv. Mater.* **20,** 4547–4551 (2008).
5. Law, M., Greene, L. E., Johnson, J. C., Saykally, R. & Yang, P. Nanowire Dye-Sensitized Solar Cells. *Nat. Mater.* **4,** 455–459 (2005).
6. Xu, S. *et al.* Ordered Nanowire Array Blue/near-UV Light Emitting Diodes. *Adv. Mater.* **22,** 4749–4753 (2010).
7. Gogurla, N., Sinha, A. K., Santra, S., Manna, S. & Ray, S. K. Multifunctional Au-ZnO Plasmonic Nanostructures for Enhanced UV Photodetector and Room Temperature NO Sensing Devices. *Sci. Rep.* **4,** 6483 (2014).
8. Anantachaisilp, S. *et al.* Tailoring Deep Level Surface Defects in ZnO Nanorods for High Sensitivity Ammonia Gas Sensing. *J. Phys. Chem. C* **118,** 27150–27156 (2014).
9. Janotti, A. & Van de Walle, C. G. Fundamentals of Zinc Oxide as a Semiconductor. *Reports Prog. Phys.* **72,** 126501 (2009).
10. Clark, S. J., Robertson, J., Lany, S. & Zunger, A. Intrinsic Defects in ZnO Calculated by Screened Exchange and Hybrid Density Functionals. *Phys. Rev. B* **2010,** *81*, 115311.
11. Wang, X. J., Vlasenko, L. S., Pearton, S. J., Chen, W. M. & Buyanova, I. A. Oxygen and Zinc Vacancies in as-Grown ZnO Single Crystals. *J. Phys. D. Appl. Phys.* **42,** 175411 (2009).
12. Stehr, J. E. *et al.* Zinc-Vacancy–Donor Complex: A Crucial Compensating Acceptor in ZnO. *Phys. Rev. Appl.* **2,** 021001 (2014).
13. T-Thienprasert, J. *et al.* Compensation in Al-Doped ZnO by Al-Related Acceptor Complexes: Synchrotron X-Ray Absorption Spectroscopy and Theory. *Phys. Rev. Lett.* **110,** 055502 (2013).
14. Look, D. C. *et al.* Self-Compensation in Semiconductors: The Zn Vacancy in Ga-Doped ZnO. *Phys. Rev. B* **84,** 115202 (2011).
15. Stehr, J. E. *et al.* Turning ZnO into an Efficient Energy Upconversion Material by Defect Engineering. *Adv. Funct. Mater.* **24,** 3760 (2014).
16. Chen, S. L. *et al.* Efficient Upconversion of Photoluminescence via Two-Photon Absorption in Bulk and Nanorod ZnO. *Appl. Phys. B* **108,** 919–924 (2012).
17. Queisser, H. J. Defects in Semiconductors: Some Fatal, Some Vital. *Science* **281,** 945–950 (1998).
18. McCluskey, M. D. Point Defects in ZnO. *Semicond. Semimetals* (2015). doi: 10.1016/bs.semsem.2014.11.002
19. Tarun, M. C., Iqbal, M. Z. & McCluskey, M. D. Nitrogen Is a Deep Acceptor in ZnO. *AIP Adv.* **1,** 022105 (2011).
20. Stehr, J. E., Hofmann, D. M. & Meyer, B. K. Electron Paramagnetic Resonance and Photo-Electron Paramagnetic Resonance Investigation on the Recharging of the Substitutional Nitrogen Acceptor in ZnO. *J. Appl. Phys.* **112,** 103511 (2012).
21. Philipps, J. M. *et al.* Recharging behavior of nitrogen-centers in ZnO. *J. Appl. Phys.* **116,** 063701 (2014).
22. Lyons, J. L., Janotti, A. & Van de Walle, C. G. Why nitrogen cannot lead to p-type conductivity in ZnO. *Appl. Phys. Lett.* **95,** 252105 (2009).
23. Lany, S. & Zunger, A. Generalized Koopmans density functional calculations reveal the deep acceptor state of N_O in ZnO. *Phys. Rev. B* **81,** 205209 (2010).
24. Tsukazaki, A. *et al.* Repeated Temperature Modulation Epitaxy for P-Type Doping and Light-Emitting Diode Based on ZnO. *Nat. Mater.* **4,** 42–46 (2004).
25. Yuan, G. D. *et al.* P-Type ZnO Nanowire Arrays. *Nano Lett.* **8,** 2591–2597 (2008).
26. Lautenschlaeger, S. *et al.* Optical Signatures of Nitrogen Acceptors in ZnO. *Phys. Rev. B* **85,** 235204 (2012).
27. Soudi, A., Khan, E. H., Dickinson, J. T. & Gu, Y. Observation of Unintentionally Incorporated Nitrogen-Related Complexes in ZnO and GaN Nanowires. *Nano Lett.* **9,** 1844–1849 (2009).
28. Herring, N. P., Panchakarla, L. S. & El-Shall, M. S. P-Type Nitrogen-Doped ZnO Nanostructures with Controlled Shape and Doping Level by Facile Microwave Synthesis. *Langmuir* **30,** 2230–2240 (2014).
29. Lu, M.-P., Lu, M.-Y. & Chen, L.-J. P-Type ZnO Nanowires: From Synthesis to Nanoenergy. *Nano Energy* **1,** 247–258 (2012).
30. Li, J., Wei, S.-H., Li, S.-S. & Xia, J.-B. Design of Shallow Acceptors in ZnO: First-Principles Band-Structure Calculations. *Phys. Rev. B* **74,** 081201 (2006).
31. Yamamoto, T. & Katayama-Yoshida, H. Solution Using a Codoping Method to Unipolarity for the Fabrication of P-Type ZnO. *Japanese J. Appl. Physics, Part 2 Lett.* **38,** L166 (1999).
32. Liu, L. *et al.* P-Type Conductivity in N-Doped ZnO: The Role of the N_{Zn}-V_O Complex. *Phys. Rev. Lett.* **108,** 215501 (2012).
33. Stehr, J. E. *et al.* Defects in N, O and N, Zn Implanted ZnO Bulk Crystals. *J. Appl. Phys.* **113,** 103509 (2013).
34. Lambrecht, W. R. L. & Boonchun, A. Identification of a N-Related Shallow Acceptor and Electron Paramagnetic Resonance Center in ZnO: N_2 on the Zn Site. *Phys. Rev. B* **87,** 195207 (2013).
35. Stehr, J. E., Meyer, B. K. & Hofmann, D. M. Magnetic Resonance of Impurities, Intrinsic Defects and Dopants in ZnO. *Appl. Magn. Reson.* **39,** 137–150 (2010).
36. Cartier, E., Stathis, J. H. & Buchanan, D. A. Passivation and Depassivation of Silicon Dangling Bonds at the Si/SiO 2 Interface by Atomic Hydrogen. *Appl. Phys. Lett.* **63,** 1510–1512 (1993).
37. Miller, D. J. & Haneman, D. Electron-Paramagnetic-Resonance Study of Clean and Oxygen-Exposed Surfaces of GaAs, AlSb, and Other III-V Compounds. *Phys. Rev. B* **3,** 2918–2928 (1971).
38. Hofmann, D. *et al.* Hydrogen: A Relevant Shallow Donor in Zinc Oxide. *Phys. Rev. Lett.* **88,** 045504 (2002).
39. Carlos, W. E., Glaser, E. R. & Look, D. C. Magnetic Resonance Studies of ZnO. *Phys. B Condens. Matter.* **308-310,** 976–979 (2001).
40. Stehr, J. E. *et al.* Defect Properties of ZnO Nanowires Revealed from an Optically Detected Magnetic Resonance Study. *Nanotechnology*. **24,** 015701 (2013).
41. Diarra, M., Niquet, Y. M., Delerue, C. & Allan, G. Ionization energy of donor and acceptor impurities in semiconductor nanowires: Importance of dielectric confinement. *Phys. Rev. B.* **75,** 045301 (2007).
42. Xu, H., Rosa, A. L., Frauenheim, T. & Zhang, R. Q. N-doped ZnO nanowires: Surface segregation, the effect of hydrogen passivation and applications in spintronics. *Phys. Status Solidi b.* **247,** 2195–2201 (2010).
43. Chen, C. Y. *et al.* Probing Surface Band Bending of Surface-Engineered Metal Oxide Nanowires. *ACS Nano*. **6,** 9366–9372 (2012).
44. Gutjahr, J., Sakong, S. & Kratzer, P. Interplay of Hydrogen Treatment and Nitrogen Doping in ZnO Nanoparticles: A First-Principles Study. *Nanotechnology* **25,** 145204 (2014).
45. Haffad, S., Samah, M. & Cicero, G. Effect of nitrogen impurities on the physical properties of ZnO nanowires: First-principles study. *Phys. Rev. B*. **85,** 165207 (2012).
46. Green, M. L. *et al.* Oxygen and carbon incorporation in low temperature epitaxial Si films grown by rapid thermal chemical vapor deposition (RTCVD). *J. Electron. Mater.* **19,** 1015–1019 (1990).
47. Sturm, J. C., Schwartz, P. V., Prinz, E. J. & Magee, C. W. Control of oxygen incorporation and lifetime measurement in $Si_{1-x}Ge_x$ epitaxial films grown by rapid thermal chemical vapor deposition. *Proc. SPIE* 1393, 252 (1991).
48. Lai, G. Y. High-Temperature Corrosion and Materials Applications (ed. Lai, G. Y.) 67–96 (ASM International, 2007).
49. Marzouki, A. *et al.* Structural and optical characterizations of nitrogen-doped ZnO nanowires grown by MOCVD. *Mater. Lett.* **64,** 2112–2114 (2010).
50. Gao, J., Zhang, X., Sun, Y., Zhao, Q. & Yu, D. Compensation mechanism in N-doped ZnO nanowires. *Nanotechnology*. **21,** 245703 (2010).

Acknowledgments

Financial support by the Swedish Research Council(VR) (Grant No. 621-2010-3971), Linköping Linnaeus Initiative for Novel Functional Materials (LiLI-NFM) supported by the Swedish Research Council (contract number 2008-6582), the ÅForsk Foundation (Grant No. 15-433) and World-Class University Program through NRF grant funded by the Korea government (MEST) (grant # R31-10026) is greatly appreciated.

Author Contributions

N.K.R. grew the samples under supervision of C.W.T. J.E.S. performed the EPR experiments and analyzed the data. J.E.S., W.M.C. and I.A.B. wrote the manuscript.

Additional Information

Competing financial interests: The authors declare no competing financial interests.

How to cite this article: Stehr, J. E. *et al.* Efficient nitrogen incorporation in ZnO nanowires. *Sci. Rep.* **5**, 13406; doi: 10.1038/srep13406 (2015).